EFFICIENT METHODOLOGY FOR LONG TERM FORECASTING OF THE SOLAR RESOURCE: A CASE STUDY FOR CALIFORNIA'S CENTRAL VALLEY

Ricardo Marquez – rmarquez3@ucmerced.edu
Carlos F.M. Coimbra – ccoimbra@ucmerced.edu
University of California Merced, Mechanical Engineering and Applied Mechanics, Merced, CA 95340-3222, United States

Abstract. *We develop a long-term solar irradiance forecasting model by adopting predicted meteorological variables from the U.S. National Weather System (NWS) forecasting database data as inputs. We evaluate the solar resource in Merced, which is centrally located between Bakersfield and Sacramento, at the heart of California's central valley (Merced is also very close to the geographical center of the state of California). An important component of our study is the development of a set of criteria for selecting relevant inputs for the forecasting model. We select variable inputs using a version of the Gamma test for stochastic modeling. In all, eleven inputs are considered, nine of which are meteorological variables, while the other two depend on solar geotemporal quantities. The solar geotemporal variables are found to be critically important, while the most relevant meteorological variables include sky cover,probability of precipitation, and maximum and minimum temperatures. A secondary objective of our study is to assess model quality as a function of both forecast horizon and seasonal dependence. For Global Horizontal Irradiance (GHI), the relative Root-Mean-Square-Error (rRMSE) is shown to be stable and relatively flat for 5-day ahead forecasts when calculated over the entire data set (a period of over a year). For Direct Normal Irradiance (DNI), the rRMSE increases by over 15% after 5 days. When the rRMSEs are calculated using monthly averages, the results show that model quality is best (lowest rRMSEs) during the months of March through September (7 months). These results are important because the highest quality of forecast results coincide with peak demand of power for the region. Prediction intervals are also derived based on regression of the squared residuals on the input variables; in this way, the model quality dependency on sky conditions is obtained. This information is also important because, as results on the monthly RMSEs suggest, forecastability depends strongly on local weather conditions and on seasonal variations.*

Keywords: *Global Horizontal Irradiation, Direct Normal Irradiation, Solar Irradiation Forecasting, Gamma Test Model Input Selection*

1. INTRODUCTION

A major obstacle for the development of adequate policies to promote and take advantage of existing solar technologies is the lack of reliable data for ground solar irradiance (both direct normal and global horizontal). Although the radiation that reaches the outer layers of the atmosphere is well defined and can be easily calculated, the solar irradiance that reaches the ground level where solar collectors (thermal and photovoltaic) operate depends strongly on localized and complex atmospheric conditions. Cloud cover, aerosol content, and the presence of participating gases in the lower atmosphere (water vapor, carbon dioxide) and in the stratosphere (ozone) can reduce the availability of direct insolation at the ground level to a small fraction of the solar irradiance that reaches the upper atmosphere. These effects are particularly strong on the Direct Normal Irradiance (DNI). Because cloud cover corresponds to the strongest effect on ground insolation, no statistical method that ignores micro-scale (> 2 km) or meso-gamma scale (2–20 km) weather systems can succeed in estimating real-time and/or forecasting solar power availability. From the operational standpoint, the balancing of supply and demand peaks in the electrical grid requires detailed consideration of the availability of solar power as California embraces a more renewable profile of energy utilization. Forecasting the available insolation is therefore an enabling technology for the success of any policy to include solar power as an important contribution to both centralized and decentralized systems.

To address this need, the National Renewable Resource Data Center (NRReDC) (http://rredc.nrel.gov/solar) developed an impressive 10-year program (1995-2005) aimed on mapping solar irradiance for the entire United States. The more recent SWERA program (http://swera.unep.net) combines many of the previously developed databases into a worldwide model for solar irradiance. The major limitation of these available databases is the fact that there is no real time solar irradiance information, and therefore no forecasting capability. In addition to these two critical limitations, the current services rely on mechanistic models and satellite image processing to estimate DNI and total solar irradiance for very extensive areas that were never actually compared against ground measurements. These models (see e.g. Bird and Hulstrom (1981); Cano et al. (1986); Gautier et al. (1980); Iqbal (1983); Schillings et al. (2004a,b)) are poorly validated against high-quality ground data, and therefore the accuracy of the satellite maps is compromised (error estimates are of the order of 20%, according to NREL reports).

Hourly meteorological predictions are produced and assembled by the National Weather System's (NWS's) national digital forecasting database (NDFD) for seven days from which it is possible to construct solar irradiation forecasts. Perez et al. (2007) have recently developed and validated forecasting models for GHI where the input variables include sky cover from NDFD and GHI_{clear} from satellite-based models. Their forecasting models were

applied in Sacramento and New York and it was found that the model accuracies were consistent with preliminary analysis with Multiple Output Statistics and meso-scales models elsewhere (e.g. Heinemann, D. (2004)). Their models were also validated against single-point stations located in Desert Rock, Nevada, Fort peck, Montana, Boulder, Colorado, Sioux Falls, South Dakota, Bondville, Illinois, Goodwin Creek, Mississippi, and Penn State, Pennsylvania (Perez et al. (2009)). These locations cover a wide range of climatic environments, and therefore the these previous studies show that potential to construct meteorological-based forecasting models is quite promising.

This study considers the use of additional meteorological variables in order to enhance the forecasting capabilities of the meteorological prediction based models. For the construction of predictive models it is desirable to know which inputs are relevant. Knowledge of the relevant inputs will not only be useful for guidance on the construction of the predictive models but will also ultimately make more efficient use of resources that go into the collection, processing and storage of the required data sets. The Gamma test is useful in this regard. The Gamma test is an algorithm designed to provide an estimate of the lowest possible MSE attainable by a smooth model for some output, y, based on the inputs, x. The criteria for choosing the content in x is then based on keeping the dimension of x small (to remove insignificant inputs), meanwhile retaining a low estimate for the MSE. The Gamma test is a relatively simple algorithm to apply and is used here as a basis for the selection of relevant inputs. The selection procedure will also involve a genetic algorithm search in order to sift through possible input combinations in a computationally efficient way.

2. DATA

DNI information is traditionally available through two distinct experimental methods: the first is direct measurement at the ground level using Normal Incident Pyrheliometers (NIPs) mounted on Solar Trackers (STs); the second involves the indirect determination of DNI by subtracting the diffuse irradiance from the global irradiation. In the second case, the diffuse radiation is obtained by blocking the direct solar beam with either a shadow band or a shadow disk (in the case of the shadow band, the data collected must be corrected for the additional band of sky that is blocked). In principle, with a Precision Spectral Pyranometer (PSP) equipped with a Shade Disk Kit (SDK) one is able to determine both components that make up the global solar irradiance (DNI and diffuse). However, SDK systems do not replicate absolute radiometer results with the same accuracy and precision of NIPs. (include info on UV and IR sensors)

The UC Merced solar observatory is equipped with three solar instruments used in this study: 1 PSP (Precision Spectral Pyranometer) for benchmarking the global irradiance, 1 NIP (Normal Irradiance Pyrheliometer), and 1 SDK (Shaded Disk Kit) mounted on a solar tracker (we will use Eppley's ST-3 solar tracker, which allows for mounting 3 instruments on a single tracker) that shades another PSP. The redundant DNI data taken by each station is statistically treated in order to detect outliers and to increase the confidence level of the measurements. In addition, each observatory is equipped with Doppler anemometers and independent T108/109 thermocouples, as well as other UV and IR instruments. Data acquisition, logging and processing is automated with the aid of a robust data-logger (Campbell ScientificÕs CR1000). The data sampling rate is 1 sample every 30 seconds from which hourly averages are calculated.

The National Weather Service (NWS) manages the National Digital Forecast Database (NDFD) which provides gridded digital forecasts of weather parameters for the entire country at high resolutions of up to 2.5-km spatial and 1-hour temporal (Glahn and Ruth, 2003; Perez et al., 2007). Local forecasts from NWS Weather Forecast Offices (WFOs) are generated by national model outputs, mesoscale model runs and human input. These local forecasts are then merged and assembled on a national grid (Glahn and Ruth, 2003; Perez et al., 2007). Weather forecasted values are publicly available and can be accessed electronically in Extensible Markup Language (XML) format through the NWS web-site: http://www.weather.gov/ndfd (Schattel and Bunge, 2008). The forecasted meteorological elements provided by the NWS include ambient temperature, dew-point temperature, relative humidity, sky cover, wind speed and direction, and probability of precipitation, significant wave height, weather type, and snow amount.

Meteorological data is collected daily (approximately at noon) for the period of this study. The data set of meteorological data collected on each day contains forecasted values for that same-day and forecasted values for the next six days. An input selection strategy based on residual variance estimation and neural networks is applied to construct solar irradiance forecasting models based on the same-day forecasts. After the predictive models have been constructed, forecasted meteorological values of the next days are inserted into the models to obtain forecasts for lead times of up to 6 days.

3. MODEL INPUTS AND INPUT SELECTION

To develop our irradiation forecasting models, eleven variables are considered for use as inputs. Nine of these variables are predicted meteorological variables (as described in Section 2). The other two variables are geometric/temporal variables: the cosine of the zenith angle, $\cos Z$, and the normalized hour angle, $\bar{\omega}$. The geometric variables are important because they describe the deterministic diurnal variations of clear-sky solar irradiation. One of the objectives of this work is to make a determination of which inputs are most useful for predicting solar irradiation and which ones can be discarded to prevent over complication of forecasting model. In order to do so, a model input selection procedure is used to determine relevant inputs. The procedure depends on the Gamma test, a non-linear analysis tool which provides an estimate of the MSE for input/output model. With a total of eleven inputs there are

$2^{11} - 1 = 2047$ possible subsets of inputs to perform the Gamma test with. Instead of evaluating all possible combinations, a genetic algorithm search is employed to explore the best subsets of inputs. The Gamma test is described in the next section followed by a description of the genetic algorithm search procedure.

Tab. 1 gives the input variables that will be used for the solar radiation models. For brief notation, the input variables will be represented as x_j where j is the associated variable number indicated in the first column of Table 1. The set of input variables consists of the meteorological variables from the weather source described in section 2, and the solar geometry variables: $\cos Z$ and ω. To avoid scaling issues that can complicate the Gamma test or neural network training, all meteorological input variables are normalized by subtracting the variables by their corresponding minimum values, then dividing by their range (maximum - minimum); in this way the values vary from 0 to 1. The maximum and minimum values used for each input variable are also listed in Tab. 1.

Table 1. Inputs for Modeling

VARIABLE NUMBER	VARIABLE NAME	MINIMUM	MAXIMUM
1	Maximum Temperature (C)	7.22	40.55
2	Temperature (C)	-2.78	40.55
3	Dew point temperature (C)	0	37.78
4	Relative Humidity (%)	0	100
5	Sky Cover (%)	0	100
6	Wind Speed (m/s)	0	22.5
7	Wind Direction (deg)	0	350
8	Probability of Precipitation (%)	0	100
9	Minimum Temperature (C)	-2.78	22.22
10	$\cos(Z)$ (dimensionless)	0	1
11	Normalized hour angle, $\bar{\omega}$ (dimensionless)	0	1

3.1 Dimensionless time scale as an input

This work introduces an additional input for modeling solar irradiance. The input considered is the normalized hour angle defined as

$$\bar{\omega} = \omega / (\omega_{max}), \tag{1}$$

where ω is known as the hour angle and ω_{max} is equal to absolute value of the maximum hour angle for a particular day while the sun is up; $\omega_{max} = \omega_{sunset} = -\omega_{sunrise}$. These variables are commonly used for standard time to solar time conversions and can be calculated by using equations given by Duffie and Beckman (2006). By definition $\omega = 0$ at solar noon which is when the sun is at it's highest elevation and when the extraterrestrial solar irradiation is at it's highest intensity. Observations of DNI daily profiles for clear-sky conditions including all parts of the year are shown in Fig. 1 for different values of $\bar{\omega}$. Fig. 1 shows that $\bar{\omega}$ is a potentially useful input variable because clear-sky DNI profiles for any part of the year have the same basic shape.

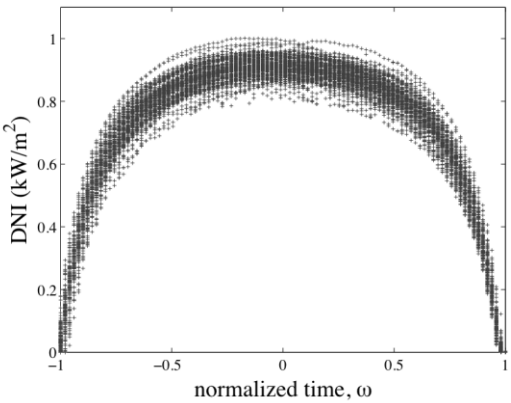

Figure 1 - DNI for clear-sky conditions plotted versus normalized time index ω. DNI profiles have same basic shape when viewed on this time scale for all parts of the year.

3.2 Residual variance estimation: Gamma test

The Gamma test was developed by Koncar, N. (1997); Stefansson et al. (1997, and further advanced by Evans and Jones (2002) and Jones (2004). The idea behind the Gamma Test is to suppose there exists a smooth model for output, y, which is based on some m-dimensional input vector, x, and has the general form

$$y = f(x) + r, \tag{2}$$

where the residual term, r, is produced by uncertainty or noise, and has a mean of 0 with variance σ_r^2.

The procedure of the Gamma test is to first construct the k^{th} $(1 \le k \le p)$ nearest neighbor list $x_{N[i,k]}(1 \le i \le M)$ of input vectors $x_i(1 \le i \le M)$, where p is the maximum number of nearest neighbors (typically $p = 10$) and M is the number of data points. The following steps are then applied:

• for $(1 \le k \le p)$ compute:

$$\delta_M(k) = 1/M \sum_{i=1}^{M} |x_{N[i,k]} - x_i|^2, \tag{3}$$

and

$$\gamma_M(k) = 1/(2M) \sum_{i=1}^{M} |y_{N[i,k]} - y_i|^2. \tag{4}$$

• construct the linear regression for relationship for the data $(\delta_M(k), \gamma_M(k))$:

$$\gamma_M(k) = \Gamma + A\delta_M(k). \tag{5}$$

Provided that the regression line is a good fit, the intercept of Eq. (5), Γ, provides a close estimate of the residual variance σ_r^2 and therefore the lowest attainable MSE. This condition is satisfied when $M \to \infty$ as proven in Evans and Jones (2002). The slope, A, gives a crude estimate of the complexity of the unknown surface of the regression function, f, we seek to model. The Gamma test is non-parametric technique and the results apply regardless of the particular methods used to subsequently build a model. This test is particularly suited for the analysis of non-linear regression problems.

An extension of the Gamma statistic, Γ is the V_{ratio}, defined as $V_{ratio} = \Gamma/Var(y)$ which is a normalization of the expected MSE. From this definition we have an parameter which is analogous to the commonly used model quality parameter, R^2:

$$R^2 \approx 1 - V_{ratio}. \tag{6}$$

Throughout this paper, we use the V_{ratio} as the Gamma test output.

When a sequence of Gamma tests are performed for an increasing number of data points it is referred to as an M-test (Jones (2004)). The M-test is useful because allows one to evaluate the reliability of the Γ as an estimate of σ_r^2, and to determine whether enough data is available for model construction. In other words, if the M-Test graph stabilizes then we can have some confidence that the Γ estimate is reasonably accurate and the problem will be relatively simple to model because the data is sufficiently dense everywhere. In Section 3.4, the M-test will be applied to verify that enough training data is available and to compare different model inputs.

For a fuller discussion on the Gamma test and the applications for modeling we refer the reader to the reference Jones (2004).

3.3 Genetic Algorithm Search for Model Input Selection

The selection of the optimal subset of inputs can be accomplished with genetic algorithms. Genetic algorithms are optimization search techniques inspired by the process of biological evolution. The algorithms involve optimization searching patterns where alleles (features) of individuals in a population of potential solutions are altered by crossover and mutation operators over generations/cycles so that the fittest individuals continue to reproduce Wilson04. In the current problem of input selection, the individual fitness is based on minimizing the objective function adopted from Durrant, P.J. (2001) and Wilson et al. (2004), which consist of three penalty terms:

$$J(x_i) = w_\Gamma f_\Gamma(x_i) + w_A f_A(x_i) + w_L f_L(x_i). \tag{7}$$

The components of the objective function f_Γ and f_A are functions of the Gamma test outputs for a subset of inputs x_i. The term f_L is the ratio of number of inputs in x_i to total number of inputs. When selecting the most relevant subset of inputs, $x_i \subset x$, the objective function encourages competition among three competing quality measures; that is, the best subset of inputs should 1) produce low prediction errors (the Γ value the subset should be small); 2) keep the complexity of the input and output relationship low (or to keeping the complexity estimate: A, small); 3) be optimal so that irrelevant features are removed. Correspondingly, The fitness scaling parameters in this objective function which need to be modified include: 1) intercept fitness weight, w_Γ; 2) gradient fitness weight, w_A; and 3) length fitness weight, w_L.

Table 2. Genetic Algorithm Search parameters for model input selection

GA PARAMETERS	VALUES
Population size	100
Crossover rate	0.5
Mutation rate	0.05
Intercept fitness, w_Γ	1
Gradient fitness, w_A	0.1
Length fitness, w_L	variable
Run time(s)	600

The term of the objective function with multiplied by w_Γ corresponds to the value of the gamma statistic, Γ, i.e., the estimate of the residual variance. In choosing a combination of inputs, it is desirable to keep the gamma statistic low, therefore, the weight for this term in the objective is kept at a high value in order to encourage retaining inputs which provide low values of Γ in the genetic algorithm search.

As mentioned in Section 3.2, the gradient is returned by the Gamma test as a crude estimation of the complexity of the model, f. At this point, we imposed no requirements on the complexity of the model to be determined, so the weight for this term in the objective function is assigned a low value of $w_A = 0.1$.

The length fitness parameter, w_L corresponds to the number of inputs to be considered in the model. The value to assign for w_L is not as straight forward because too little emphasis on the length fitness leads to the retention of insignificant or counterproductive inputs. On the other hand, too much emphasis on the length fitness may lead to an overall increase in the gamma statistic for the population of inputs in the genetic algorithm search. Therefore, the length fitness is left as a variable and subsets of inputs are considered based on which inputs remain relevant as the length fitness is increased from 0.1 to 1.

3.4 Evaluation of Input Selection

The genetic algorithm optimization search is applied using the winGamma computer software. The length fitness parameter, w_L, is varied from 0.1 to 1 and the results obtained by the genetic algorithm search are used to produce the bar plots in Figs. 3a and 3b where the height of the bars represent the frequency (in percent) that each input is included in the best 10% of input subsets which minimized the objective function. These results indicate that the variable x_{10} ($\cos Z$) is the most important input for modeling GHI. This is expected because $\cos Z$ dictates the deterministic part of the global horizontal solar irradiation. The next most relevant inputs for GHI are x_5, x_8, and x_9. The variables which seem to be the least important are x_7, and x_4 which have no frequency in the best 10% of input combinations.

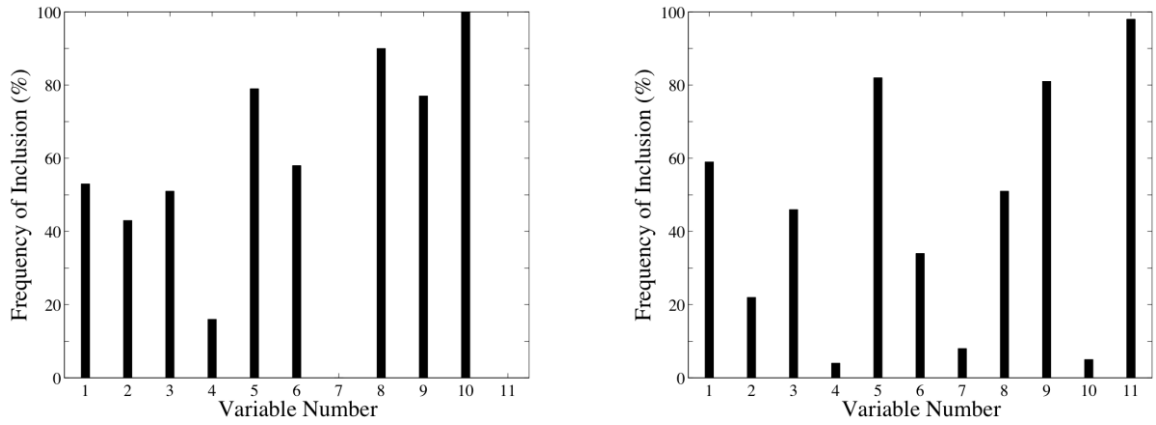

a) GHI b) DNI

Figure 2 - Genetic Algorithm results for model input selection. High frequency of inclusion indicates that the variable is useful for minimizing the objective function, Eq. (7).

Fig. 2 can be used for choosing a few input subsets to develop forecasting models. Based on Fig. 2a, the combination of inputs to be considered and analyzed for GHI are subset 1: [x_8, x_{10}]; subset 2: [x_5, x_9,x_8, x_{10}]; subset 3: [x_1, x_2, x_3, x_5, x_6, x_8, x_9, x_{10}] and subset 4: [all variables]. The inputs in subset 1 corresponds to the two variables which are predicted by the genetic algorithms to have the most significance. The combinations of inputs in subset 2 includes the variables in subset 1 but additionally including the next significant variables: x_5 and x_9. Inputs set 3 increments subset 2 by including the additional variables which appear to have some relevance, x_1, x_2, x_3, and x_6. We also consider model construction with all the variables.

The relevant inputs for DNI are slightly different than for GHI. The most relevant inputs appear to be x_5, x_9,

and x_{11}. The four subsets selected for modeling DNI are subset 5: [x_5, x_9, x_{11}], subset 6: [x_1, x_3, x_5, x_8, x_9, x_{11}], subset 7: [x_1, x_2, x_3, x_5, x_6, x_8, x_9, x_{11}], and again subset 4: [all variables].

An M-Test is performed on the selected inputs and the results are plotted in Fig. 3. As described in Section 3.2 the reliability of the Gamma Test can be inferred from the stability of the M-Test plots. All GHI M-test plots appear to have stabilized indicating that enough data is obtained and that the Gamma test results are reliable. It is clear that the variables x_8 and x_{10} will probably not be enough to obtain the most accurate models. The M-test results for DNI are similar in that the variables x_5, x_9, and x_{11} will not give the best possible model accuracy.

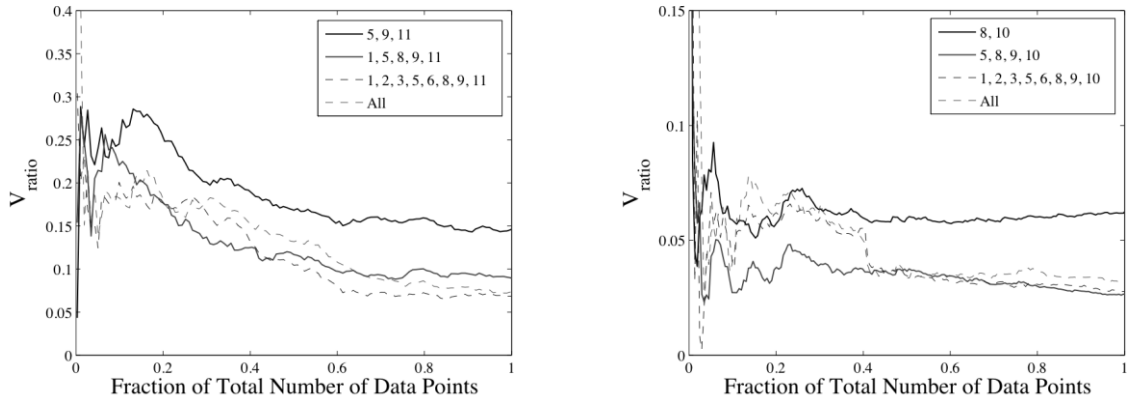

a) GHI b) DNI

Figure 3 - M-Tests for various input subsets that were selected based on results obtained from GA results. The V_{ratio} on the vertical axis is an estimate of the normalized MSE, i.e. $\approx 1 - R^2$. The total number of data points for GHI is 4472 and for DNI is 3738.

4. ARTIFICIAL NEURAL NETWORKS

An artifical neural network (ANN) is a particular representation of y in terms of some input variables x. The ANN representation is based on signals being sent through elements called neurons in such a way that the processing of the inputs signals produces an output, y, that is sufficiently close to the desired target value of t. Neurons are arranged in layers, where the first layer contains the set of inputs, the last layer contains the output, and the layers in between, referred to as hidden layers, contain hidden neurons. A feedforward ANN with m inputs and N_l neurons in one hidden layer can be expressed as

$$y = f(x, w) = f_2\left(\sum_{q=1}^{N_l} w_{2,q} f_1\left(\sum_{j=1}^{m} w_{1,qj} x_j + w_{1,0}\right) + w_{q,0}\right). \tag{8}$$

In Eq. 8, f_1 is the activation function in the hidden layer and f_2 is the activation in the output layer. The neurons in the input layer do no processing. A characteristic of feedforward ANNs is that the neurons are successively interconnected from layer to layer where neurons in one layer affect all neurons in the next but do not affect other neurons in the same layer or any preceding layers. Numerical optimization algorithms such as back-propagation, conjugate gradients, quasi-Newton, and Levenberg-Marquard have been developed to efficiently adjust the weights, $w_{1,qj}$ and $w_{2,q}$ in the feedforward ANNs so that the minimization of some performance function is achieved. Typically the performance function used for adapting the weights is the MSE.

$$\text{MSE} = \frac{1}{M}\sum_{i=1}^{M} (y_i - t_i)^2. \tag{9}$$

ANNs are useful tools for approximating complicated mapping functions for problems in classification and regression (Bishop, 1994), and have also been used extensively in many areas including solar radiation modeling. Mellit (2008) gives a review of over 40 applications of neural networks and other artificial intelligence techniques applied to solar radiation modeling. The advantage of ANNs is that no assumptions are required about the underlying process relating input and output variables. However, because ANNs are universal approximating functions, their mapping capabilities can potentially lead to problems such as overfitting the data (Bishop, 1994), and thus leading to poor generalization on new data sets. To avoid overtraining, we use the Gamma test results as an indication of how far to train the neural networks as is done in (Moghaddamnia et al. (2009); Remesan et al. (2008)) as well as making sure that the ANN MSEs on training data and test data closely match.

5. MODEL DEVELOPMENT AND EVALUATION

The ANN models were constructed using MATLAB Neural Network Toolbox version 6.0.4. The input data for the regression consists of same-day forecasted meteorological variables. Data for same-day forecasting were randomized and split into two categories consisting of a training set and a test set. The proportions of each set are based on the results of the M-test (Fig. 3). Accordingly, the training set consists for 60% of the randomly selected points of the entire data set to train the GHI neural networks and 80% to train the DNI neural networks. The neural network architectures are based on the feedforward structure described in Section 4 where the input layer consist of the inputs from the four subsets suggested in Section 3.4 and where the number of neurons used for modeling were kept relatively low, ranging from 10 to 40, depending if any significant improvements in model accuracy (low MSE) was noticed. The weights are adapted using Levenberg-Marquard learning algorithm and the stopping criteria for neural network training is based on continued to training until the R^2 reaches the Gamma test output, $1 - V_{ratio}$, or for a maximum of 100 training cycles.

5.1 Forecasting Model Results

The eight models differed by their inputs as is indicated in Table 5.1 and 3. The model quality measures used for comparisons of the different models include the R^2, RMSE, and relative RMSE (rRMSE), which are calculated using the following equations:

$$R^2 = 1 - \frac{\sum_{i=1}^{M} (y_i - \hat{y}_i)^2}{\sum_{i=1}^{M} (y_i - \bar{y}_i)^2} \tag{10}$$

$$RMSE = \sqrt{\frac{1}{M} \sum_{i=1}^{M} (y_i - \hat{y}_i)^2} \tag{11}$$

$$rRMSE = RMSE / \bar{y} \tag{12}$$

In the above equations, $\hat{y}_i$ is the predictions for the ANNs, y_i, are measured values of GHI or DNI, and $\bar{y}$ are the averages of GHI or DNI for the training or test set.

Eight predictive models were trained and tested to forecast solar irradiation. Models 1 - 4 forecast GHI and Model 5 - 8 forecast DNI. Each of the ANN models were trained for 100 training cycles using 12 to 20 neurons in the hidden layer. When more neurons were used, larger discrepancies of model statistics between the training and testing sets were observed and thus the models generalized more poorly.

By comparing the statistical measures for training and test sets of each model, we notice there is are significant improvements over the simpler models with the least inputs. As is often the case in modeling with neural networks, better training performance is achieved when more inputs are used. However, using more inputs does not necessarily translate to better generalization or ability to forecast. The results in Tabs. 3 and 4 show that models with intermediate complexity perform the best on both training and test sets. Persistent models for GHI and DNI are also shown in the tables. These persistent models represent the situation that the previous day's solar irradiance hourly profile closely matches the next days profiles as would be the case for consecutive sunny days. Comparing the ANN models (1 through 8) with the persistent models clearly shows that the improvement of the ANN models, especially for DNI forecasting.

Table 3. Training and testing results for GHI.

		TRAINING			TEST		
Model	Inputs	RMSE(kW/m^2)	rRMSE(%)	R^2	RMSE(kW/m^2)	rRMSE(%)	R^2
1	$[x_8, x_{10}]$	0.077	19.3	0.939	0.089	22.8	0.915
2	$[x_5, x_8, x_9, x_{10}]$	0.067	17.2	0.952	0.072	17.7	0.947
3	$[x_1, x_2, x_3, x_5, x_6, x_8, x_9, x_{10}]$	0.063	15.7	0.959	0.073	18.5	0.945
4	[All]	0.058	14.8	0.965	0.074	18.6	0.942
Persistent		-	-	-	0.107	24.5	0.867

Table 4. Training and testing results for DNI.

		TRAINING			TEST		
Model	Inputs	RMSE(kW/m^2)	rRMSE(%)	R^2	RMSE(kW/m^2)	rRMSE(%)	R^2
5	$[x_5, x_9, x_{11}]$	0.171	35.0	0.763	0.162	32.3	0.781
6	$[x_1, x_3, x_5, x_8, x_9, x_{11}]$	0.142	29.1	0.835	0.156	31.2	0.801
7	$[x_1, x_2, x_3, x_5, x_6, x_8, x_9, x_{11}]$	0.148	30.1	0.821	0.161	33.2	0.788
8	$[All]$	0.138	28.1	0.845	0.158	32.0	0.797
Persistent		-	-	-	0.244	56.7	0.458

It is also interesting to compare results from Tabs. 3 and 4 with the M-test results in Figs. 3a and 3b. In comparing the actual training R^2s of each model with those predicted from the M-tests, we see that they are quite close, in particular, for the GHI models. For example, according to the M-test for Model 1, we could have expected an $R^2 \approx 0.945$, which is close to the actual $R^2 = 0.939$. The training R^2s for GHI are generally much closer to what was predicted in the M-test than for DNI. This is likely because the M-test plots have stabilized with a relatively smaller proportion of data at $\approx$ 45% as compared to DNI where the M-test plots do not stabilize until after $\approx$ 80% of total number of data points used, and as a result GHI is much easier to predict than DNI and which also means that more data will be required to obtain better models for DNI.

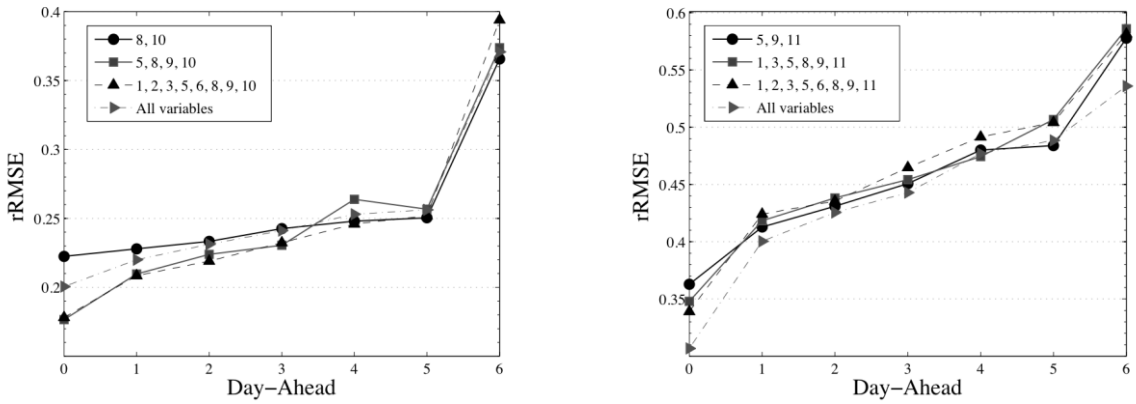

a) GHI b) DNI

Figure 4 - The relative RMSE (%) for forecasts using models with different inputs as indicated in the legend on graph. The horizontal axis represents the number of days ahead where 0 denotes same-day.

One concern for using a greater number of inputs is that prediction errors of each inputs would directly propagate to errors in forecasting the outputs. In order to observe whether this would happen, forecasting errors for all models for same-day and several days ahead are shown in Figs. 4a and 4b. The legends show the input variables associated with each model. These figures illustrate how forecasting errors increase with increasing forecasting lead-times. Two general observation from these figures are that models with less inputs have lesser nominal increases in forecasting errors, and DNI is much more difficult to predict. Also, as forecasting horizon increases there is less of a difference between the models, and therefore the preferred models would be Model 1 and Model 5 because less inputs are involved.

The rRMSEs given so far are a measure of model quality over the entire data set. In some cases it may be important to know if there are certain periods when the solar radiation is more predictable. The rRMSEs for GHI Model 3 and DNI Model 7 are calculated on a monthly basis to produces Figs. 5 and 6. For both models the rRMSEs are lower than the aggregated rRMSE during the months between and including March through September. It is also apparent from these figures that during the summer months solar irradiation is much more forecastable.

5.2 Prediction Intervals

As a post-analysis step, prediction intervals are provided in order to gauge how model and forecasting uncertainty depends the type of sky situation. For instance, as shown in Figs. 5 and 6, model and forecasting accuracy is generally much better during summer months when there are few cloudy days. References such as Bacher et al. (2009) and Lorenz et al. (2009) have constructed prediction intervals based on analysis of the residual distributions. In a similar manner, prediction intervals are constructed here by analyzing the residuals as described next.

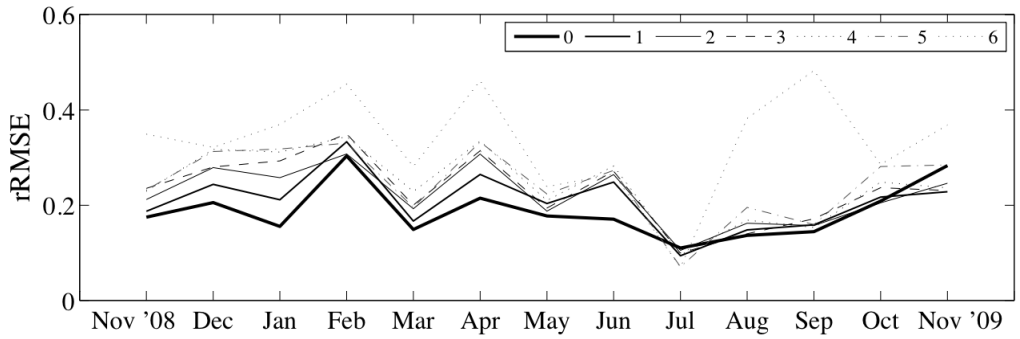

Figure 5 - The relative RMSE by month from beginning of November 2008 to end of November 2009. The rRMSEs are normalized with respect to $GHI_{mean} = 0.4741 kW/m^2$. The rRMSEs are for modeling GHI for same-day and forecasts one to six-days ahead as indicated by legend on graph.

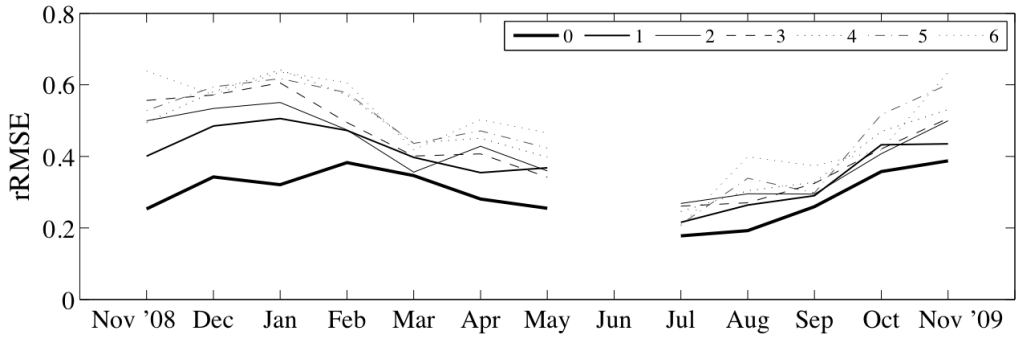

Figure 6 - The relative RMSE by month from beginning of November 2008 to end of November 2009. The rRMSEs are normalized with respect to $DNI_{mean} = 0.541 kW/m^2$. The rRMSEs are for modeling DNI for same-day and forecasts one to six-days ahead as indicated by legend on graph. June data is deemed unreliable due to mechanical problems with tracking system.

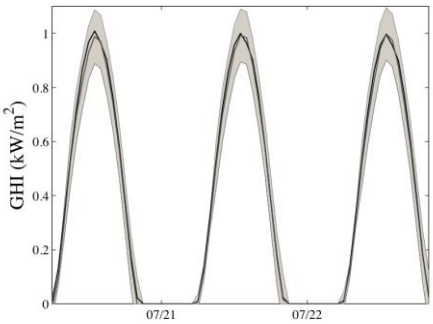

a) Same-day forecasts clear days

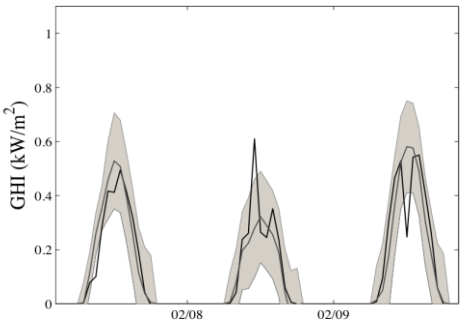

b) Same-day forecasts non-clear days

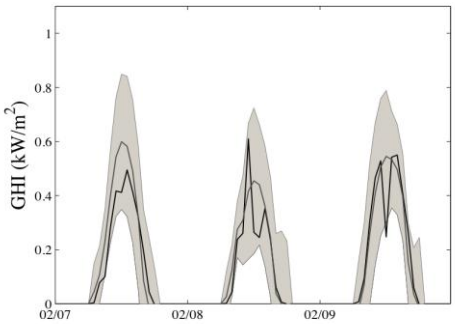

c) One-day Ahead forecasts non-clear days

Figure 7 - Forecasts with prediction intervals for hourly GHI. The dark-bold lines are the measured values, the grey lines are the predictions, and the shaded regions are the 95% confidence intervals.

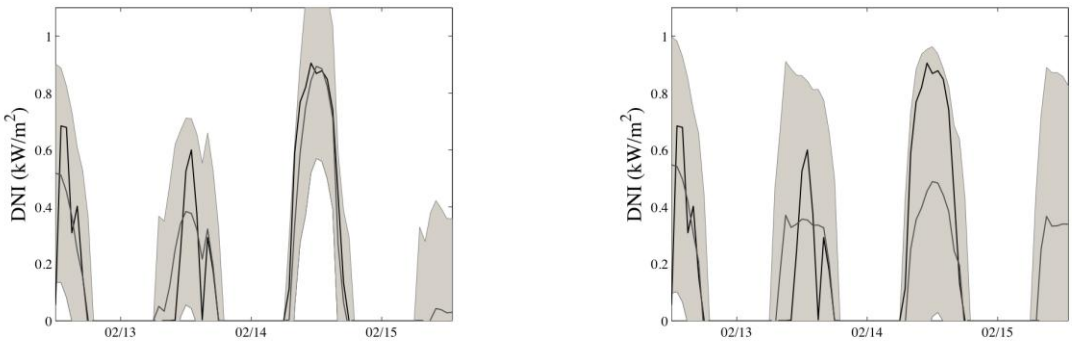

a) Same-day Forecasting b) One-day Ahead Forecasting

Figure 8 - Forecasts with prediction intervals for hourly DNI. The dark-bold lines are the measured values, the grey lines are the predictions, and the shaded regions are the 95% confidence intervals.

Fig. 7 show time-series plots of GHI and modeled GHI with the corresponding prediction bands. For clear days, Fig. 7a, the prediction bands are relatively narrow indicating that GHI is very predictable for clear sky situations. Non-clear days are much less predictable as indicated by the wider prediction bands, as shown in Fig. 7b. Fig. 7c shows one-day ahead predictions of GHI for the same days in Fig. 7b showing that GHI uncertainty does not increase much more in the one-day ahead forecasting horizon than the same-day uncertainty. The larger forecasting uncertainty during partly cloudy to overcast conditions for single-point model prediction are consistent with the findings of Bacher et al. (2009) and Lorenz et al. (2009). One can also compare the prediction intervals for same-day forecasts with 1-day ahead forecasts for DNI in Fig. 8. The prediction intervals for DNI are much wider then for GHI which further illustrates that DNI is much more difficult to predict reliably. These plots give a fuller illustration of the predictability of solar irradiance from the meteorological data based models than the summary statistics such as R^2 and RMSE would be able to give alone.

6. CONCLUSIONS

We developed hourly solar irradiation forecasting models using artificial neural networks for lead times of up to six days. Model inputs included predicted meteorological data obtained from the National Weather Services forecasting database, and solar geometry variables. The normalized hour angle was introduced as a potential input for modeling solar irradiation. Employing the Gamma test and auxiliary genetic algorithms revealed that the relevant inputs include the solar geometry variables, sky cover, probability of precipitation, and minimum and maximum temperatures. Minimum and maximum temperatures may be important because these variables help to account for seasonal dependencies on solar irradiation and cloud cover relationships.

Model quality measures such as the relative RMSE (rRMSE) for the same-day forecasts show that the models constructed here are comparable to those of satellite-based models (Perez et al. (2002), Schillings et al. (2004b), Vignola et al. (2007)), and other medium-range (one to six-days ahead) forecasting models (Lorenz et al. (2009), Bacher et al. (2009), Breitkreuz et al. (2009)). For same-day forecasts of GHI, rRMSE's range from 15 to 22% for different models constructed on 13 month data set. Forecasting DNI is much more difficult: rRMSEs obtained on same-day forecasts are in the range of 28 to 35%. In general, the models lose accuracy as the forecasting horizon is increased but less sharply during the summer than during the winter months. This is due to long periods of consecutive clear days in the summer and a large number of cloudy to overcast days during the winter.

Because the forecasted meteorological is available freely from NWS, these types of solar irradiation models can be developed anywhere in the United States. Additionally, these models can be easily extended to produce solar irradiation maps in cases where regional studies of the solar resource is of interest. Although satellite-based models could serve the same purpose, satellite-based models do not have any direct forecasting capabilities. On the other hand, the forecasting based models could be used to store simulated solar irradiation records when using the more accurate same-day forecasted values.

REFERENCES

Bacher, P., Madsen, H., Nielsen, H. A., 2009. Online short-term solar power forecasting. Solar Energy 83, 1772–1783.

Bird, R., Hulstrom, R., August 1981. Review, evaluation, and improvement of direct irradiance models. Transactions of the ASME. Journal of Solar Energy Engineering 103, 182–192.

Bishop, C., 1994. Neural networks and their application. Review of Scientific Instruments 65, 1803–1832.

Breitkreuz, H., Schroedter-Homscheidt, M., Holzer-Popp, T., Dech, S., 2009. Short-range direct and diffuse irradiance forecasts for solar energy applications based on aerosol chemical transport and numerical weather modeling. Journal of Applied Meteorology and Climatology 48, 1766–1779.

Cano, D., Monget, J., Albuisson, M., Guillard, H., Regas, N., WALD, L., 1986. A method for the determination of the global solarradiation from meteorological satellite data. Solar Energy 37, 31–39.

Duffie, J. A., Beckman, W. A., 2006. Solar Engineering of Thermal Processes, Third Edition . John Wiley & Sons, Inc., Hoboken,New Jersey.

Durrant, P.J., 2001. winGammaTM: a non-linear data analysis and modelling tool for the investigation of non-linear and chaotic systems with applied techniques for a flood prediction system. Ph.D. thesis, Department of Computing Science, Cardiff University.

Evans, D., Jones, A., 2002. A proof of the Gamma test. Proceedings of the Royal Society of London Series A-Mathematical Physical and Engineering Sciences 458, 2759–2799.

Gautier, C., Diak, G., Masse, S., 1980. A simple physical model to estimate incident solar radiation at the surface from goes satellite data. Journal of Applied Meteorology 19, 1005–1012.

Glahn, H., Ruth, D., 2003. The new digital forecast database of the national weather service. Bulletin of the AmericanMeteorological Society 84, 195–201.

Heinemann, D., 2004. Forecasting of solar irradiation. In: Proceedings of the International Workshop of Solar Resource from the Local Level to Global Scale in Support of the Resource Management of Renewable Electricity Generation, Institute for Environment and Sustainability, Joint Research Center, Ispra, Italy.

Iqbal, M., 1983. Introduction to solar radiation. Academic Press, Toronto, Ont., Canada.

Jones, A., 2004. New tools in non-linear modelling and prediction. Computational Management Science 1, 109–149.

Koncar, N., 1997. Optimisation methodologies for direct inverse neurocontrol. Ph.D. thesis, Department of Computing Imperial College of Science, Technolgoy and Medicine, University of London.

Lorenz, E., Hurka, J., Heinemann, D., Beyer, H. G., 2009. Irradiance forecasting for the power prediction of grid-connected photovoltaic systems. IEEE Journal of Selected Topics in Applied Earth Observations and Remote Sensing 2, 2–10.

Mellit, A., 2008. Artificial Intelligence technique for modelling and forecasting of solar radiation data: a review. International Journal of Artificial Intelligence and Soft Computing 1, 52–76.

Moghaddamnia, A., Remesan, R., Kashani, M. H., Mohammadi, M., Han, D., Piri, J., 2009. Comparison of LLR, MLP, Elman, NNARX and ANFIS Models-with a case study in solar radiation estimation. Journal of Atmospheric and Solar-Terrestrial Physics 71, 975–982.

Perez, R., Ineichen, P., Moore, K., Kmiecik, M., Chain, C., George, R., Vignola, F., 2002. A new operational model for satellite-derived irradiances: Description and validation. Solar Energy 73, 307–317.

Perez, R., Kivalov, S., J., S., Hemker, K. J., Renne, D., Hoff, T., 2009. Validation of Short and Medium Term Operational Solar Radiation Forecasts. ASES Annual Conference, Buffalo, New York.

Perez, R., Moore, K., Wilcox, S., Renne, D., Zelenka, A., 2007. Forecasting solar radiation - Preliminary evaluation of an approach based upon the national forecast database. Solar Energy 81, 809–812.

Remesan, R., Shamim, M. A., Han, D., 2008. Model data selection using gamma test for daily solar radiation estimation. Hydrological Processes 22, 4301–4309.

Schattel, Jr., J. L., Bunge, R., 2008. The national weather service shares digital forecasts using web services. Bulletin of the American Meteorological Society 89, 449–450.

Schillings, C., Mannstein, H., Meyer, R., 2004a. Operational method for deriving high resolution direct normal irradiance from satellite data. Solar Energy 76, 475–484.

Schillings, C., Meyer, R., Mannstein, H., 2004b. Validation of a method for deriving high resolution direct normal irradiance from satellite data and application for the Arabian Peninsula. Solar Energy 76, 485–497.

Stefansson, A., Koncar, N., Jones, A., 1997. A note on the Gamma test. Neural Computing & Applications 5, 131–133.

Vignola, F., Harlan, P., Perez, R., Kiniecik, M., 2007. Analysis of satellite derived beam and global solar radiation data. Solar Energy 81, 768–772.

Wilson, I., Jones, A., Jenkins, D., Ware, J., 2004. Predicting housing value: Genetic algorithm attribute selection and dependence modelling utilising the Gamma test. In: Binner, JM and Kendall, G and Chen, SH (Ed.), Applications of Artificial Intelligence in Finance and Economics. Vol. 19 of Advances in Econometrics : A Research Annual. JAI-Elsevier Sci BV, Sara Burgerhartstraat. PO Box 211, 1000 AE Amsterdam, Netherlands, pp. 243–275.